

Dipartimento di Scienze e Tecnologie Aerospaziali
Politecnico di Milano

ORBITAL MECHANICS PROJECT

ROMEO SIMONE
10606804 - 970667

TESTA ALBERTO
10623874 - 888794

SCHÜTZ VIKTOR
10757226 - 962153

RESTUCCIA MASSIMILIANO
10568180 - 966289

Group 38

POLITECNICO DI MILANO



06-02-2021

Contents

1 ABSTRACT	1
Nomenclature	2
2 INTERPLANETARY MISSION	3
2.1 MISSION PRESENTATION	3
2.2 ASSUMPTIONS	3
2.3 WINDOW CHOOSING	3
2.3.1 GA ALGORITHM	4
2.3.2 GRID SEARCH	4
2.3.3 FMINCON MINIMIZATION	5
2.4 FLYBY COMPUTATION	5
2.5 RESULTS	6
2.5.1 MINIMUM ΔV ZONE	6
2.5.1.1 PORK CHOP PLOT	7
2.5.2 INTERPLANETARY LEGS	8
2.5.3 FLYBY	9
2.5.3.1 TIME OF FLIGHT ON HYPERBOLA	10
2.5.4 FINAL MISSION OVERVIEW	11
3 PLANETARY MISSION	12
3.1 PROBLEM PRESENTATION	12
3.2 NOMINAL ORBIT	12
3.3 PERTURBATIONS	13
3.3.1 J_2	13
3.3.2 SOLAR RADIATION PRESSURE	13
4 GROUND TRACK	14
4.1 GROUND TRACK REPETITION	15
5 ORBIT PROPAGATION	16
5.1 FILTERING	18
5.2 REAL ORBIT COMPARISON	19
Bibliography	20
6 APPENDIX A: PROCESS OUTPUT	21
7 APPENDIX B: SURF PLOT OF THE INTERPLANETARY LEGS	24

1. ABSTRACT

The following project consists of two independent tasks, which were solved in the frame of the *Orbital Mechanics* lecture by Prof. Camilla Colombo at the Politecnico di Milano.

The first task is about an interplanetary exploration mission from Mercury to Jupiter with a flyby-maneuvre at Mars. The goal here, is to find an optimal time window for the departure, the flyby-maneuvre and the arrival of the spacecraft. A MATLAB algorithm was developed to solve the task by using a minimization process in order to find the minimum total ΔV for the interplanetary transfer.

The second task deals with a planetary mission to analyze and understand the behavior of a Low-Earth-Orbit that is subjected to the J2 perturbation caused by the Earth, as well as the Solar-Radiation-Pressure acting on a spacecraft and hence on its orbit, caused by the photons coming from the Sun. The aim was to understand the propagation of the orbit by using two different numerical methods. The comparison of an orbit, similar to the assigned one, with real debris allowed furthermore to verify the accuracy of the implemented model.

Nomenclature

Common

AU	Astronomical unit [$1.496 \cdot 10^8 km$]
e	eccentricity

Interplanetary

ΔV	Delta Velocity [km/s]	C_R	Reflection Coefficent
μ_{Ma}	Gravitational Constant of Mars [km^3/s^2]	J_2	earth oblatness
Ω	RAAN	k	number of s/c revolutions
ω	Perigee anomaly	M	Mass of the spacecraft
θ	True anomaly	m	number of planet revolutions
f	Eccentric anomaly Hyperbola	n	Spin velocity of the Earth[rad/s]
i	inclination of the orbit [rad]	p	semi-latum rectum [km]
r_{pH}	Perigee radius of the Hyperbola	p_{sr}	SRP for unit of area at 1 AU
t	Time from perigee [s]	r	Position vector [km]
TOF	Time of flight [HH:MM:SS]	R_{Earth}	Mean radius of Earth [6378.15 km]
y	year [365.25 days]	r_{sc-Sun}	Distance spacecraft-sun [km]

Planetary

$\dot{\Omega}$	Node regression [rad/s]	SRP	Solar radiation pressure
$\dot{\omega}$	Perigee drift [rad/s]	T	Satellite orbital Period [s]

2. INTERPLANETARY MISSION

2.1 MISSION PRESENTATION

The goal of the interplanetary mission is the arrival at Jupiter, with minimizing the total cost in terms of the change of velocities during the transfer. The mission departs from Mercury and uses Mars for a flyby manoeuvre. The provided data is the minimum departure date, as well as the maximum arrival date. So in order to find the minimum cost for the mission, an optimal departure date has to be found.

2.2 ASSUMPTIONS

To solve the mission goal a few assumptions were made. One is that the two Lambert's arcs of the interplanetary trajectory are targeting directly the planet's center. This assumption can be made due to the negligible size of the sphere of influence of each planet when put into perspective to the heliocentric system. The second assumption is considering the flyby-manoeuvre as an impulsive manoeuvre according to the Restricted-Two-Body-Problem. So from the heliocentric point of view the flyby-time-window is valid for the arrival at the planet, as well as the departure from the planet. To verify this assumption, the time of flight in the sphere of influence is reported and compared with the total time of flight of the interplanetary transfer.

2.3 WINDOW CHOOSING

The first task, in order to solve the interplanetary transfer, is to choose the right time window. In this segment a process is implemented to analyze a large number of points contained in a given time range. The provided outputs are the best dates for departure, flyby and arrival. The conceptual scheme of this process is depicted in figure 2.1. So given a large time window, the GA Algorithm determines the minimum ΔV , which is then used to reconstruct a new time window. This new time window is further used for the grid search and storage of all orbit-information.

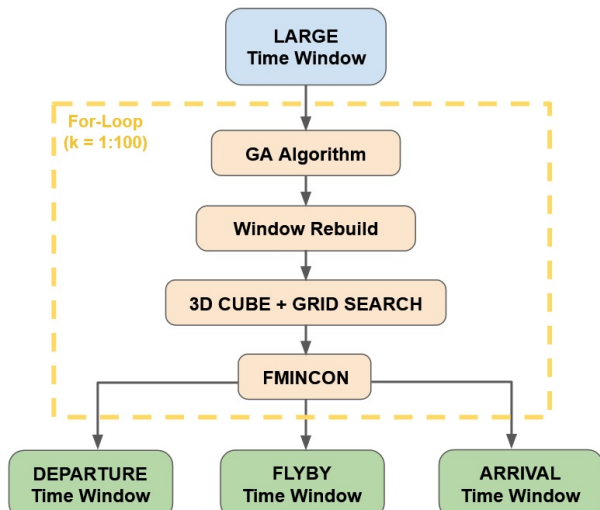


Figure 2.1: Process overview

2.3.1 GA ALGORITHM

The GA algorithm allows to set a lower and an upper boundary, which is composed of the starting day of the chosen trial window and the final date, respectively. The given time windows are presented in the following table.

Departure	Flyby	Arrival
2028/10/01-2065/01/01	2029/01/01-2066/01/01	2030/01/01-2068/10/01

The chosen approach for solving the problem was to generate as many combinations of dates for the interplanetary transfer as possible. Hence a very large time window was considered. The algorithm generates a random set of points inside this time range (here 2000), and evolves them to find the minimum of the fitness function. In our case it is the computation of the ΔV for the transfer. The GA algorithm can be very useful in helping to find the zone of minimum transfer cost. In fact its task is to reduce a given large time range considering the cost of the total mission. The GA algorithm works in combinations with a Random-Number-Generator, providing different results every time the algorithm runs. This type of problem solving approach was chosen, to decrease drastically the size of the computational time by preventing huge computations that are needed for a precise analyse of all the possible combinations of the time range. Such a computational task would be close to the impossible, given the computational power of a regular personal computer.

Another approach to this problem could be the computation of the two separate interplanetary legs in order to find the common minimum zone. However, this could lead to errors due to some missing data, while the GA Algorithm allows to investigate more combinations of the minimum zone itself.

2.3.2 GRID SEARCH

The idea behind the *Grid Search* is to create a time window, using the first computed results. The function "*Build Time Window*" was created to calculate a more precise ΔV , that is required for the transfer. It uses the computed optimal dates, provided by the GA algorithm and creates a vector with this optimal date in its middle. The length of the time span around this centered value is chosen in dependence of the orbital period of the planet. So a smaller orbital period like the one of Mercury, leads to a smaller time range around the optimal date.

Departure	Flyby	Arrival
30d - Output GA + 30d	60d - Output GA + 60d	120d - Output GA + 120d

The next step was to compute all possible ΔV s. This was done in another function called "*delta v min*" using the implemented triple nested loop and starting with the discretization of the time window. One loop of the algorithm is used to compute the ΔV , necessary for the departure from Mercury. It also provides the excess velocity for entering the sphere of influence of Mars. Another loop computes the ΔV , necessary for the rendezvous with Jupiter, as well as the total cost of the pericentre-maneuvre, that has to be performed by the spacecraft. The sum of those results is stored in a three-dimensional array, with the departure-window, the flyby-window and the arrival window each as one dimension. Using a grid search minimization process, the minimum ΔV provided by the "vectorial cube", that corresponds to 3 dates in each dimension, can be found. According to the discretization that is imposed by the process, these are the best dates for departure, flyby and arrival.

2.3.3 FMINCON MINIMIZATION

The last minimization algorithm that is used in the process, is the MATLAB-function "*Fmincon*". It uses the dates corresponding to the minimum transfer cost, that were found by the grid search, as its input. Another function, that is used, computes the minimum cost for only one set of dates and is called "*min transfer data*". Using the gradient-method for minimizing the value of the ΔV , the fmincon-process is capable of finding the local minimum of the input function.

2.4 FLYBY COMPUTATION

The powered flyby is a manoeuvre that "*steals*" some of the energy of the planet, causing the velocity vector to rotate with respect to the entry direction. This rotation modifies the magnitude of the velocity due to the different composition of the exit velocity and the planet's heliocentric velocity. Using the Lambert's arcs for the transfer between the planets, the cost for the pericentre-manoeuvre, in order to connect both arcs, can also be calculated.

The crucial parameter of the flyby is the radius of perigee of the hyperbola. On one hand, because this parameter is sufficient to fully define an interplanetary mission with a Lambert-Solver. On the other hand, this radius can be used as a constrain for the minimization process of the GA algorithm.

The functions "*Flyby Powered*" and "*Perigee Radius*" were developed to compute the flyby cost and the perigee radius by solving a non-linear equation (2.1). δ represents the total turning angle of the two semi-hyperbola.

$$\delta = \frac{\delta_-}{2} + \frac{\delta_+}{2} \quad (2.1)$$

One other condition, that has to be fulfilled, is that the altitude of the periapsis must be big enough to stay above the planet's atmosphere. If this condition is not met, the spacecraft is affected by a drag force, which in turn modifies the *eccentricity* and the *semi major axis* of the hyperbolic orbit. This leads then to a change of the escape hyperbola and in the worst case to an unwanted impact with the planet. Considering this phenomena, the radius of the periapsis for the *Flyby powered* algorithm is chosen to be the radius of Mars plus an altitude to be outside of the martian atmosphere. Knowing that the Earth's atmosphere is thicker, it can be assumed, that its influence is negligible above 200km from the planet's surface. An upper limit is also provided for the algorithm, which is the radius of the sphere of influence of the planet (Equation 2.2):

$$R_{SOI} = R_{MA-Sun} \left(\frac{M_{Ma}}{M_{Sun}} \right)^{\frac{2}{5}} \quad (2.2)$$

These constrains avoid all the numerical solutions of potential hyperbolas with a radius that is not acceptable for the model that is used to describe the problem. Another important tool is the right choice of the initial guess to solve the non-linear equation 2.1. During the test phase some numerical solutions came out to be simply the radius of atmosphere. This can be explained with the procedure of the *fzero*-function implemented in MATLAB, which finds either complex values of the radius or a very small radius of perigee. This problem can be avoided by using more accurate initial guesses, provided by computing the radius of perigee of two different non-powered flybys,

where the magnitude of the entry and exit velocity are equal relative to the planet, but different in their direction. So one radius of periapsis can be determined by using the entry velocity equaling to the first actual entry velocity. The second radius can be computed by using the magnitude of the exit velocity. The mean value of these two radii of periapsis is then the initial guess for the *fzero*-function.

2.5 RESULTS

In this chapter the focus lies on applying the method from above to compute the results of the transfer and depict graphically the orbits, as well as the zone of the minimum ΔV .

2.5.1 MINIMUM ΔV ZONE

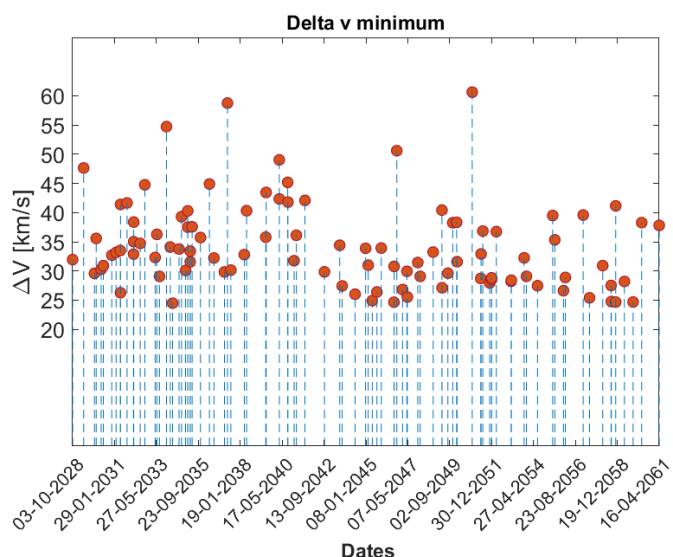


Figure 2.2: ΔV vs Departure dates from Mercury

Figure 2.2 shows the results of the minimization process described before. The *Mean Value* for the ΔV is 34.2202 km/s, with a *Standard Deviation* of 7.2931 km/s. It is clear, that there are some

minimum zones (2033-2035, 2045-2047 or 2056-2058) where a departure is likely to be efficient. These zones depend strongly on the position of Mars and Mercury with respect to Jupiter, the orbital Period T and the *Synodic Period* as shown in Table 2.1. It is also clear to see, that the period that drives the zone of minimum, where Jupiter's position creates the best window for departure, is repeating itself approximately every eleven to twelve years. Although this period is also Jupiter's orbital period, the planet's positions have to match to create an optimum.

Table 2.1: Planets and their orbital periods and synodic periods

Planet	Period [y]
Mercury	0.2408
Mars	1.8808
Jupiter	11.8668
Synodic Me-Ma	0.2762
Synodic Ma-J	2.2351
synodic Me -J	0.2458

The Best minimum ΔV -zone found by the process is shown in the following Table 2.2:

Departure window	Flyby window	Arrival Window
21/3/2034 - 20/5/2034	5/21/2038 - 4/4/2039	10/6/2041-5/2/2042

Table 2.2: Best time windows for the Interplanetary Mission

2.5.1.1 PORK CHOP PLOT

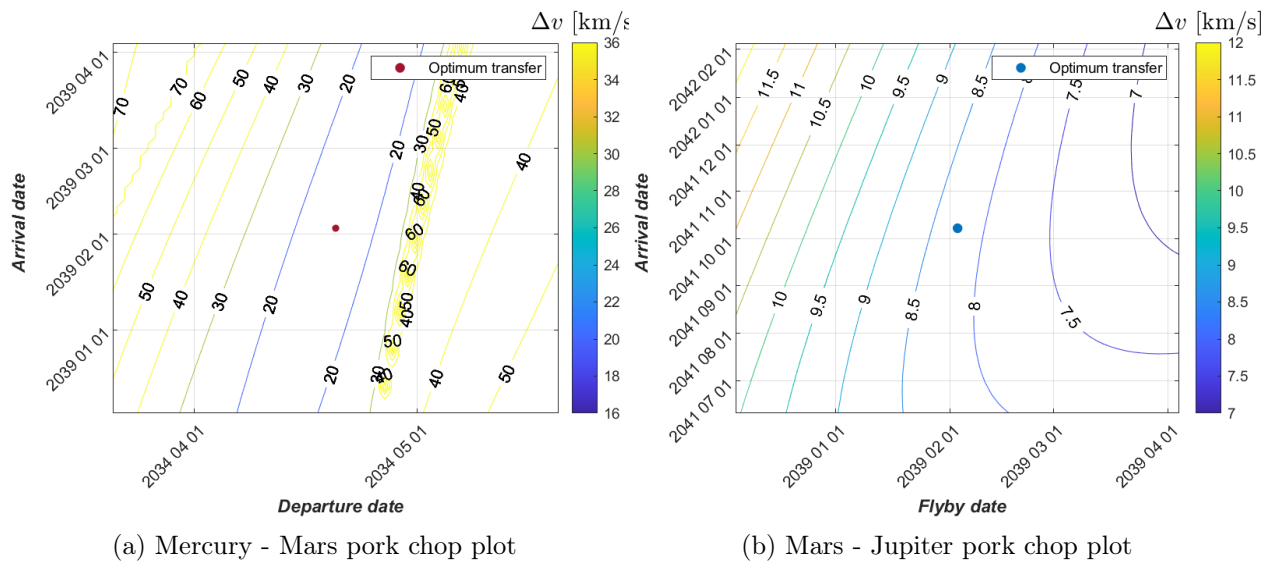


Figure 2.3: Pork Chop plots

In the figure above the pork chop plot of the two separate interplanetary legs are shown, considering only the ΔV that is actually provided by the spacecraft to go in the orbit.

It is clear, that the first transfer is the more fuel consuming one, because of the change of plane due to the high inclination of Mercury. Due to Mercury's high velocity around the sun, also a high precision is necessary in order to minimize the order to take the lowest ΔV as possible. This situation is also depicted in Figure 7.1 in the Appendix B, where the red dot indicates the chosen transfer.

This consideration above isn't valid for the second interplanetary leg, due to the low cost transfer between Mercury and Jupiter with respect to the first one. In fact, as it is shown in the Figure 7.2, the chosen orbit is not in the absolute minimum zone, which is also shown in the pork chop plot.

In the first pork chop plot it can be seen that the minimum transfer zone is very little, and the rate of change of the external part is very high. This minimum zone repeats itself according to the Synodic period of Mercury and Mars. The importance of the relative position with respect to Jupiter is comprehensible. These pork chop plot analysis proves, that the approach of considering two separate transfers, in order to find the common minimum, can be very risky.

2.5.2 INTERPLANETARY LEGS

The first interplanetary leg that is computed by the algorithm is shown in the Figure 2.4. It is a very elliptical orbit crossing the orbit of Jupiter near its apoapsis, and arriving at Mars in a position that is close to the periapsis of the orbit. According to that behaviour, the entry velocity is very high. This orbit is also inclined as it is shown in Table 2.3 due to the inclination of the Mercury's orbit. During the Test phase, some orbital shapes came out with different *semi major axis* and *eccentricities*. Sometimes Jupiter's orbit is crossed, and sometimes the apoapsis happens to be before, depending on the position of Mars and Mercury.

After the flyby, that provides only a very little change to the velocity, the orbit directed to Jupiter is almost the same as the orbit of the first interplanetary leg. In this case Jupiter is almost at the apoapsis of the transfer orbit, which provides is the optimal solution for the transfer. So the most efficient strategy can be driven, with using a transfer that start at the periapsis of the inner orbit and arrive the apoapsis of the outer.

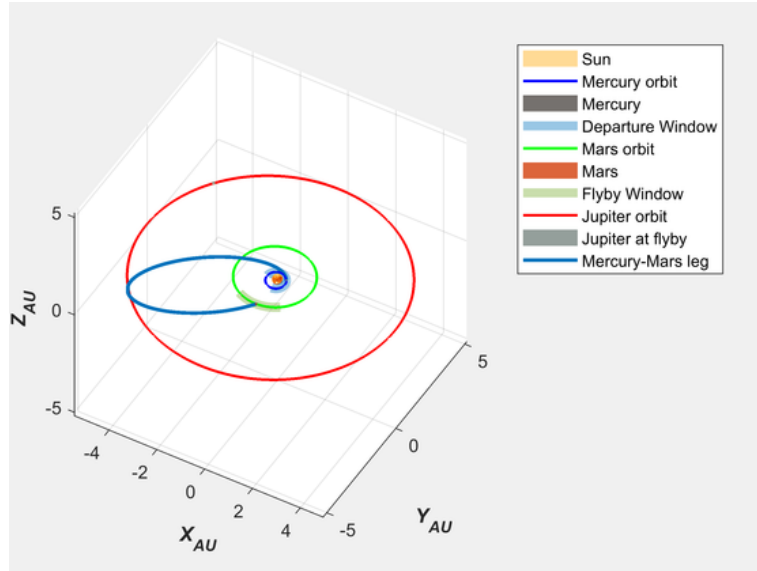


Figure 2.4: Mercury-Mars transfer orbit

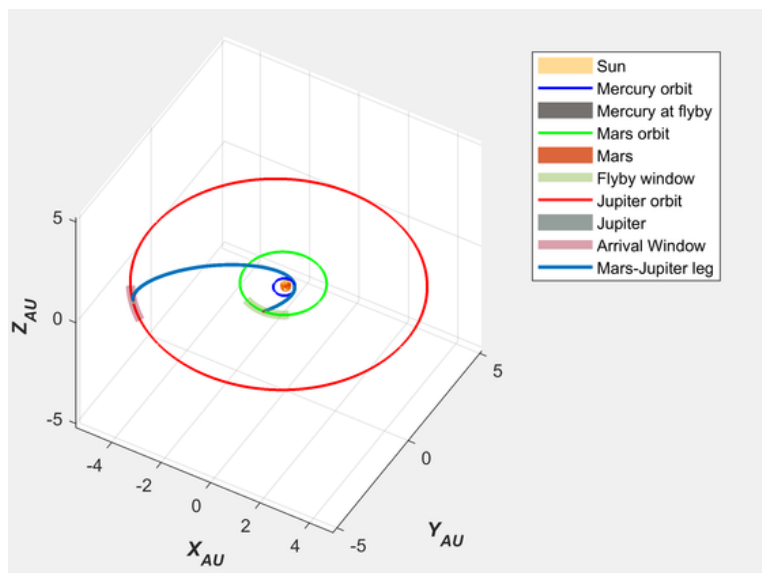


Figure 2.5: Mars-Jupiter transfer orbit

This Second interplanetary leg is passing very close to the Sun and intersecting Mercury's orbit without encountering the planet again.

For real missions the control of the spacecraft's path has to be considered, due to gravitational influences of nearby planets, like Earth and Venus, with more accurate models.

When reviewing the Keplerian elements of the orbits, one can see as well, that the *Right Ascension of the Ascending Node - RAAN* and the *Anomaly of Perigee* are very similar between the two legs. This due to the solver finding the minimum cost transfer when the planets are almost aligned.

Table 2.3: Keplerian elements of the two Interplanetary Legs

Kep. El.	Mercury-Mars	Mars-Jupiter
a_{km}	4.3593e8	4.3002e8
e	0.8882	0.8892
i_{rad}	0.0724	0.0489
ω_{rad}	1.2589	1.1170
Ω_{rad}	5.7024	5.8571

2.5.3 FLYBY

Table 2.4 shows that the flyby-hyperbolas have very high eccentricities due to the very high velocity of the spacecraft at the center of the sphere of influence. The *semi major axis* of the hyperbolas are very little due to the relative high velocity, provided at the escape from Mercury. Note that the two hyperbolas have the same inclination i , as well as a very high similarity of all other Keplerian Elements. This is due to the manoeuvre at perigee being very small.

Table 2.4: Keplerian elements of the two Hyperbolas

	Hyperbola 1	Hyperbola 2
a_{km}	-67.5584	-67.1241
e	117.0085	117.7589
i_{rad}	1.2425	1.2425
ω_{rad}	1.9082	1.9082
Ω_{rad}	4.7206	4.7206
$r_p[km]$	7837.34155	7837.34155

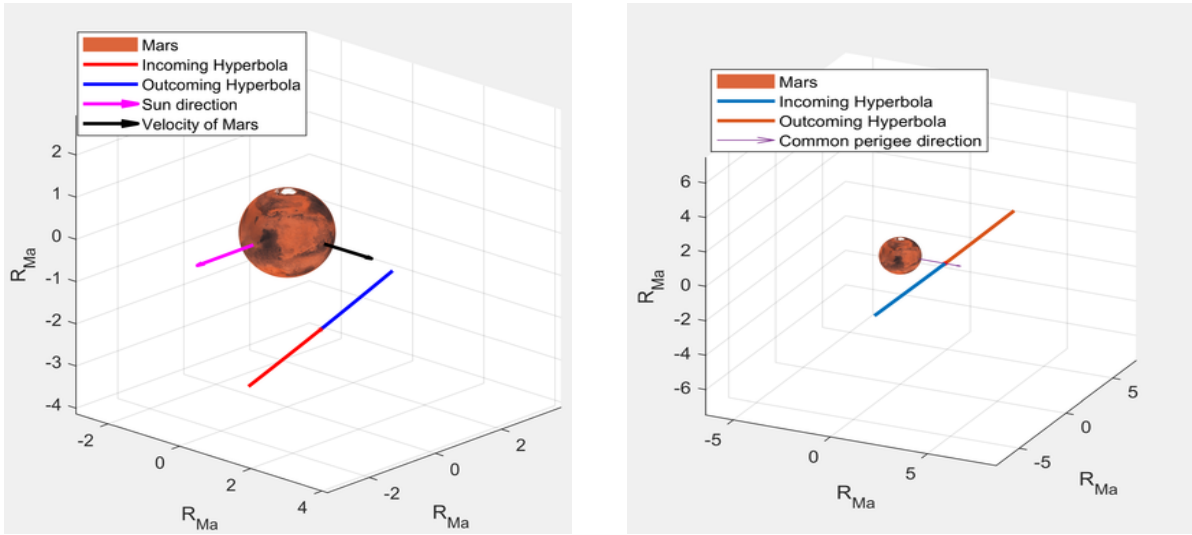


Figure 2.6: Flyby plots

2.5.3.1 TIME OF FLIGHT ON HYPERBOLA

The time of flight computation is provided by the function "*TOF powered GA*". The eccentric anomaly for the hyperbola f is defined by the following equation:

$$f = 2 \cdot \arctan \left(\sqrt{\frac{e-1}{1+e}} \cdot \tan \frac{\theta}{2} \right) \quad (2.3)$$

Knowing that the θ values are the intersection between the Mars's SOI and the hyperbola and solving the Kepler's equation to find the time of flight on the semi-hyperbola,

$$t = \sqrt{\frac{a^3}{\mu}} (f - \sinh(f)) \quad (2.4)$$

the total time of flight is:

$$\text{TOF} = 12\text{h } 42\text{m } 41\text{s} .$$

2.5.4 FINAL MISSION OVERVIEW

	ΔV [km/s]	TOF
LEG 1	16.2557	4.7912 y
FLYBY REAL	0.4373	12h 42m 41s
FLYBY POWERED	0.0806	12h 42m 41s
LEG 2	8.2474	2.6776 y
MISSION	24.4786	7.4689 y

	Date
Departure	20/04/2034
Departure	03/04/2039
Departure	08/10/2041

Table 2.5: Results

Table 2.5 shows, that the hypotheses about the cost is verified. In fact, the first interplanetary transfer is much more expensive than the second one. This is due to the escape from Mercury and the consistent plane change. The computations also show, that the flyby is a very small manoeuvre in terms of a velocity change. This can be explained with the relatively high velocity of the spacecraft, when it is entering the *SOI* of Mars. This small value is also achieved due to the choice of this particular time window, where the three planets are in a particular, almost aligned position. This leads to the almost uselessness for the spacecraft of changing the orbit, because the two interplanetary legs are very similar to each other.

The assumption of the flyby time being very little with respect to the total time of flight is also verified by the computation.

In table 2.5 also *FLYBY REAL* is added as a result with its cost and its *Time of Flight* - *TOF*. It represents the total magnitude of the flyby. However, for the total mission cost calculation, only the *FLYBY POWERED* is considered.

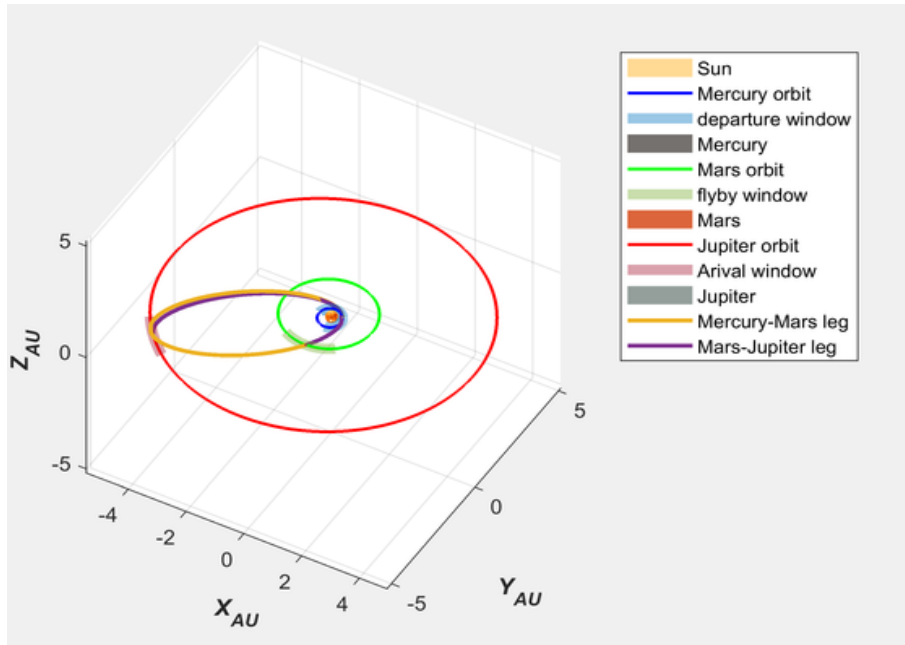


Figure 2.7: Interplanetary Mission Overview

3. PLANETARY MISSION

3.1 PROBLEM PRESENTATION

The PoliMi Space Agency wants to launch a Planetary Explorer Mission, to perform Earth observation. In this second part, it will be studied the effects of orbit perturbations on the assigned orbit. In detail, the J_2 effect and the SRP will be taken into account. Different propagation methods will be implemented and, finally, a frequency analysis will be employed.

3.2 NOMINAL ORBIT

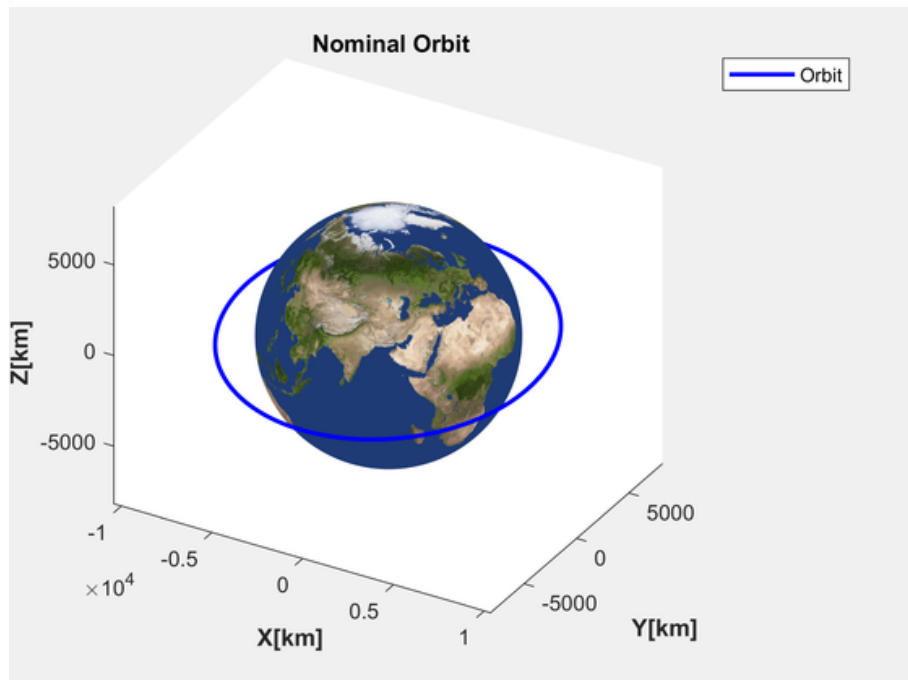


Table 3.1: Nominal orbit in Cartesian frame

The assigned orbit is a LEO, with a *semi-major axis* of 8274 km, and its shape is near to a circular orbit due to the very low *eccentricity*, to be precise 0.0053. It is a prograde orbit $0 < i < 90$ with an *inclination* of 7.8081°. The orbital period is 2h 4m 51s.

3.3 PERTURBATIONS

3.3.1 J_2

$$\vec{a}_{J_2} = \frac{3 J_2 \mu R_e^2}{2 r^4} \left[-\frac{x}{r} \left(5 \frac{z^2}{r^2} \right) \mathbf{i} + \frac{y}{r} \left(5 \frac{z^2}{r^2} - 1 \right) \mathbf{j} + \frac{z}{r} \left(5 \frac{z^2}{r^2} - 3 \right) \mathbf{k} \right] \quad (3.1)$$

The Central body perturbation is the main perturbation that a spacecraft feels during his orbital motion, the focus is on the first zonal harmonic: J_2 , that represent how much the Earth is far from a perfect sphere. The zonal harmonic model represents the variation of the mass of the earth only depending on the Geocentric distance r and the latitude ϕ , according to this it is possible to write a potential function where J_2 represent the first harmonic. The High-order harmonics like J_3 and J_4 are neglected because their magnitude is very low compared to J_2 , but in higher phase of mission design the high order harmonics has to be counted. The analysis is main focused on the secular effect J_2 which acts on the *right ascension of the ascending node, the argument of perigee* and the *true anomaly*.

$$\dot{\Omega}_{SEC} = -\frac{3nR_{Earth}^2 J_2}{2p^2} \cos i = -8.0026 \cdot 10^{-7} \text{ rad/s} \quad (3.2)$$

$$\dot{\omega}_{SEC} = \frac{3nR_{Earth}^2 J_2}{4p^2} (4 - 5 \sin^2 i) = 1.5782 \cdot 10^{-6} \text{ rad/s} \quad (3.3)$$

$$\dot{M}_{SEC} = -\frac{3nR_{Earth}^2 J_2 \sqrt{1-e^2}}{4p^2} (3 \sin^2 i - 2) = -7.8539 \cdot 10^{-7} \text{ rad/s} \quad (3.4)$$

The above sets of equations show the main effects caused by the J_2 Perturbation to the path of the spacecraft. *The Regression of the node*, $\dot{\Omega}_{SEC}$, drift westward for prograde orbits and *advance of the perigee*, $\dot{\omega}_{SEC}$, positive according to the right hand side rule.

3.3.2 SOLAR RADIATION PRESSURE

The second assigned perturbation is the Solar-Radiation-Pressure. This perturbation induces periodic variation to all the orbital elements, specially affecting a and e , in fact SRP tends to circularize the orbit periodically, causing a danger situation for the altitude of perigee that could fall into a region where the Atmospheric drag may affect seriously the path of the spacecraft. Solar Radiation Pressure effect is generally greater on smaller bodies, since they have a larger surface area to mass ratio. Over 800km altitude from the surface of the Earth SRP is greater than the atmospheric drag as it's shown in [4].

$$a_{SRP} = p_{SR@1AU} \frac{AU^2}{||r_{SC-Sun}||^2} c_R \frac{A_{SUN}}{M} \quad (3.5)$$

$$\vec{a}_{SRP} = -a_{SRP} \frac{r_{SC-Sun}}{||r_{SC-Sun}||} \quad (3.6)$$

4. GROUND TRACK

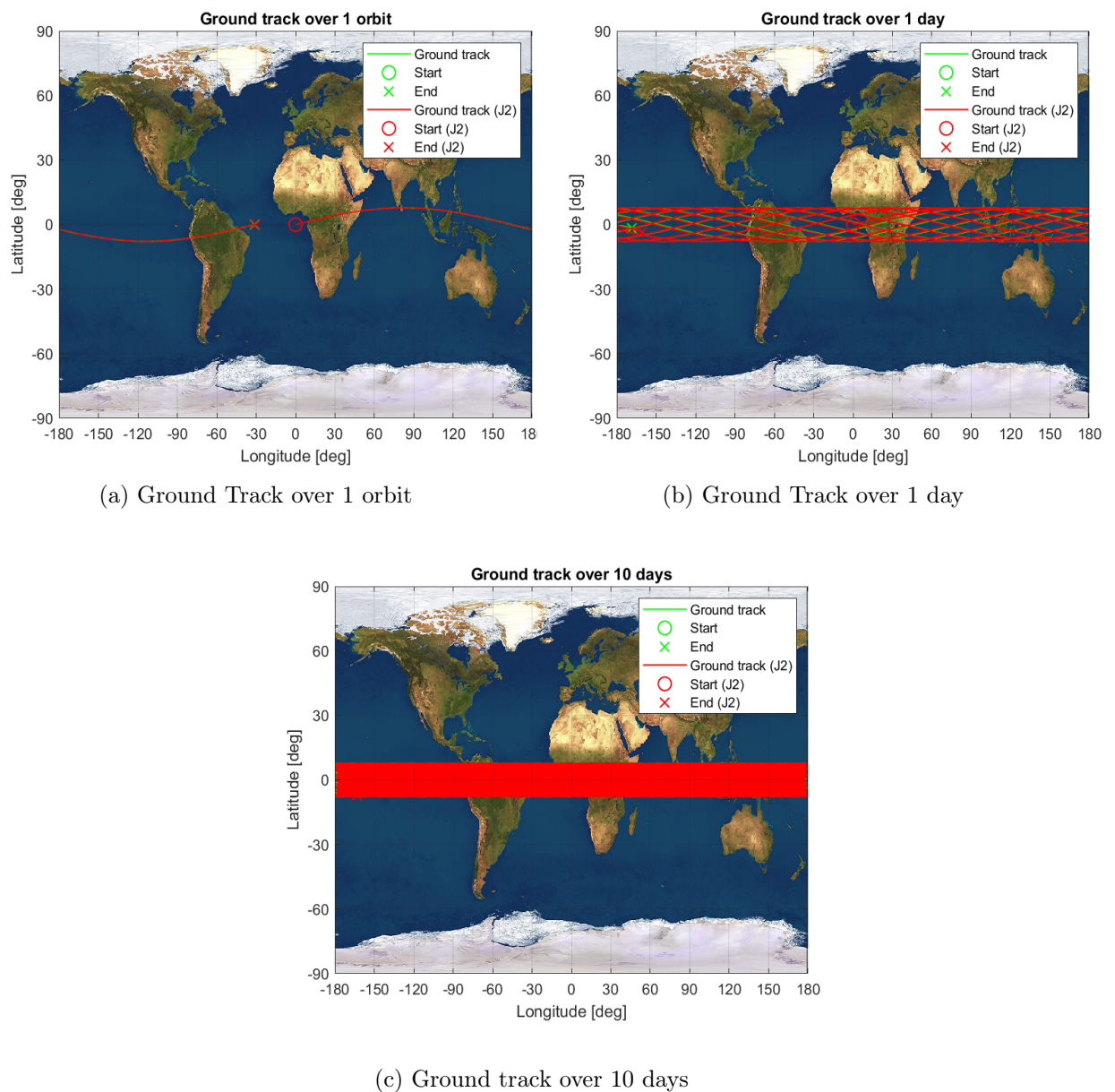


Figure 4.1: Ground Tracks

Over one orbit the ground track does not close exactly because of the rotation of the Earth. So the ground track moves westward by an angle $\Delta \lambda$. with $\omega_e = 15.04 \text{ deg/h}$

$$\Delta\lambda = T\omega_e \quad (4.1)$$

As shown in the previous point, the effects of J_2 are very small, in fact looking at Figure 4.1a appears only a very small difference. Keeping focus on Figure 4.1 it's shown that the Satellite has a coverage of the northern part of the South America, and central Africa; the altitude is low and the spacecraft is very fast so it can be used for scientific measurement or to take photo of this zone when it's Earth pointing.

4.1 GROUND TRACK REPETITION

Aiming to realize the repeating ground tracks, it is useful to introduce Equations where period change according to Equation 4.3 and 4.4 causing also a change in the *semi major axis*. In the Figures 4.2a and 4.2b we can see the difference between a simple ground track and a repeating one, where it is revealed that the repeating ground tracks closes exactly. In a real mission these two values can be computed in order to obtain the closure of the ground tracks, considering also the computation of the new semi major axis in order to obtain the repeating ground tracks. Then for a repetition with the secular J_2 effects we have to find the value of the *semi major axis* solving Equation 4.2.

$$\frac{m}{k} = \frac{\tilde{T}}{\tilde{T}_E} = \frac{\omega_E - \dot{\Omega}}{n + \dot{\omega} + \dot{M}_0} \quad (4.2)$$

$$\tilde{T} = \frac{2\pi}{n + \dot{M}_0 + \dot{\omega}} \quad (4.3)$$

$$\tilde{T}_E = \frac{2\pi}{\omega_E - \dot{\Omega}} \quad (4.4)$$

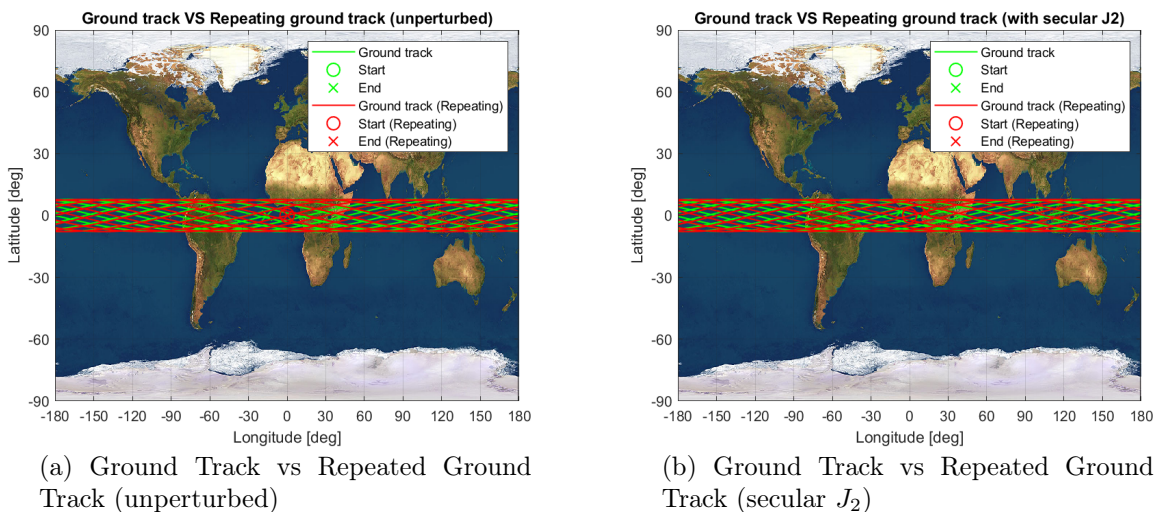


Figure 4.2: Repeated Ground Tracks comparison

5. ORBIT PROPAGATION

In order to propagate the initial orbit, and hence determine the corresponding time-evolution of the orbital elements, two different approaches will be implemented and compared: Cartesian method and Gauss method.

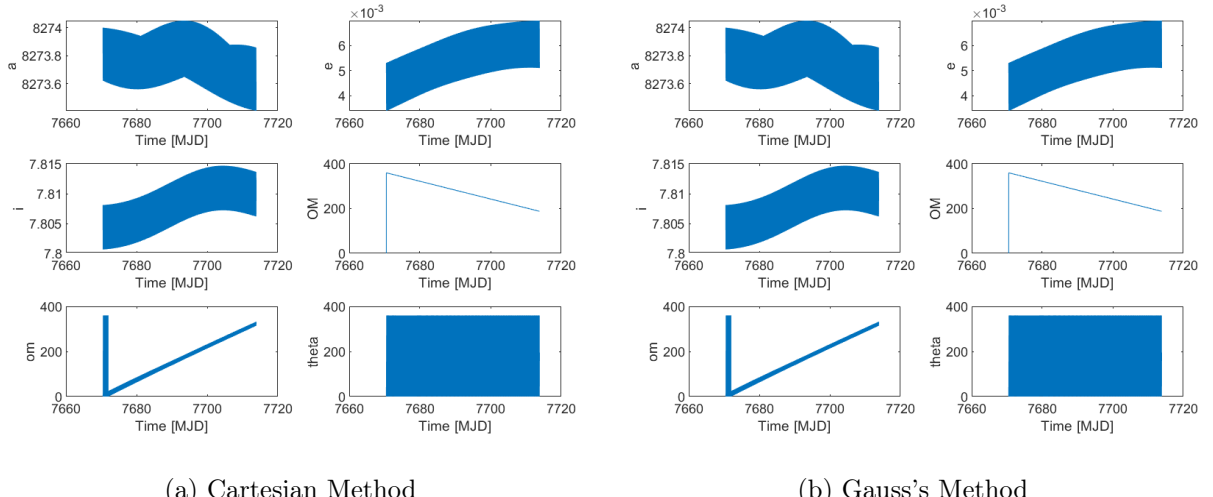


Figure 5.1: Keplerian element's variation Cartesian vs Gauss

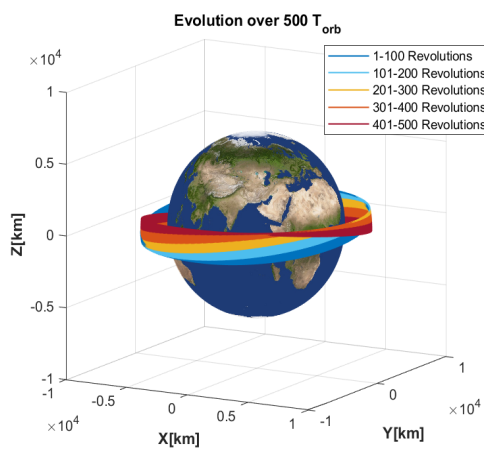


Figure 5.2: Evolution of the orbit over $500 T_{orb}$

Gauss method starts from the variation of the 6 Keplerian elements, and evaluates the evolution in time, propagating them over a large time span. Cartesian method instead builds a perturbed acceleration that is introduced into the equation of the dynamics as a disturbance and it will be integrated over the time. Each perturbation adds a term in the acceleration.

From Figures 5.1a and 5.1b it can be observed that there is a long term oscillation of e , and i due to the main effect of the SRP, and a short term oscillation of Ω and ω due to J2 effect. In Figure 5.2 it is shown how the orbits behave over 500 orbital periods, it can be seen the changes of i, Ω . The movie shows also the changes of ω and e by plotting also the eccentricity vector.

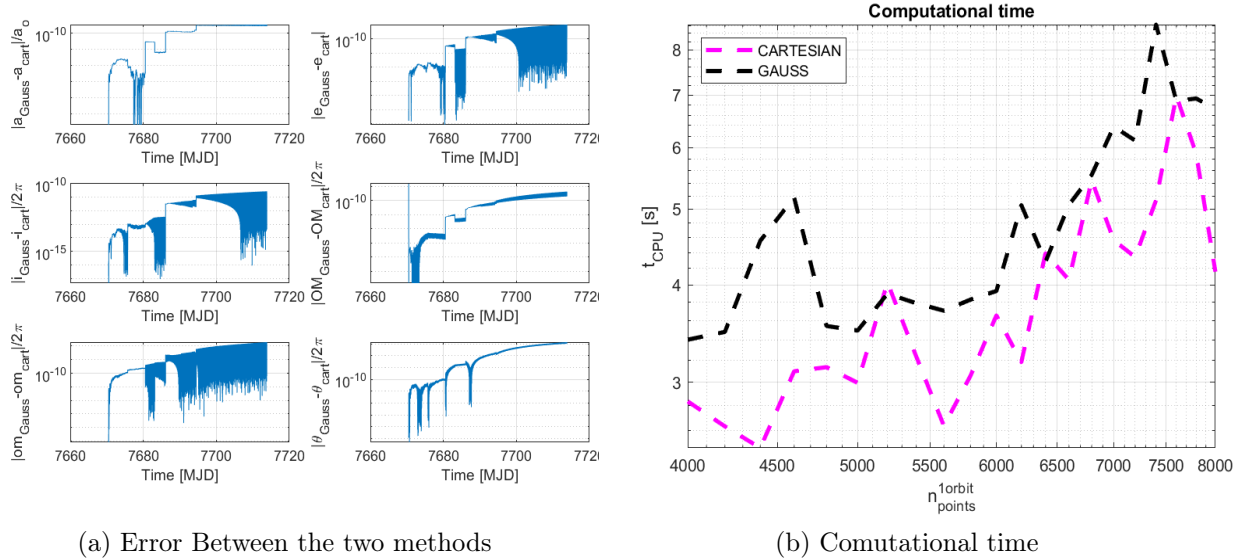


Figure 5.3: Cartesian vs Gauss

From the Figure 5.3a it can be noted that the two methods converges at the same results, as it's expected. The error fluctuates near to the Machine error of MATLAB fixed at 10^{-16} so the difference between these two method is the computational efficiency.

The above figure 5.3b shows the different computational time for the two different implemented methods, Cartesian and Gauss. It's important to note that this plot strongly depends on the performance of the PC in the time of the analysis, the cartesian method under this condition is faster than the Gauss method, but they fluctuate a lot and in some points are equal.

5.1 FILTERING

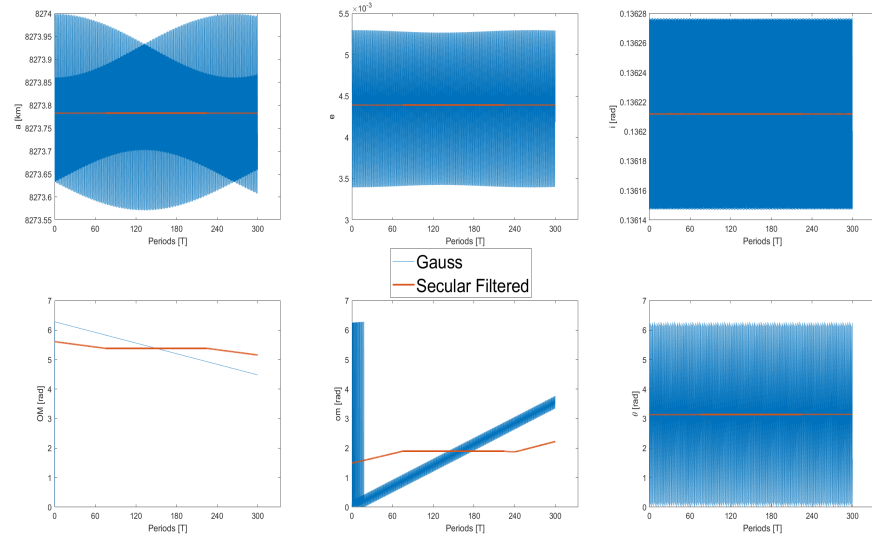


Figure 5.4: Filtering the secular effect on Gauss method, with only J_2 , over $300 T_{orb}$

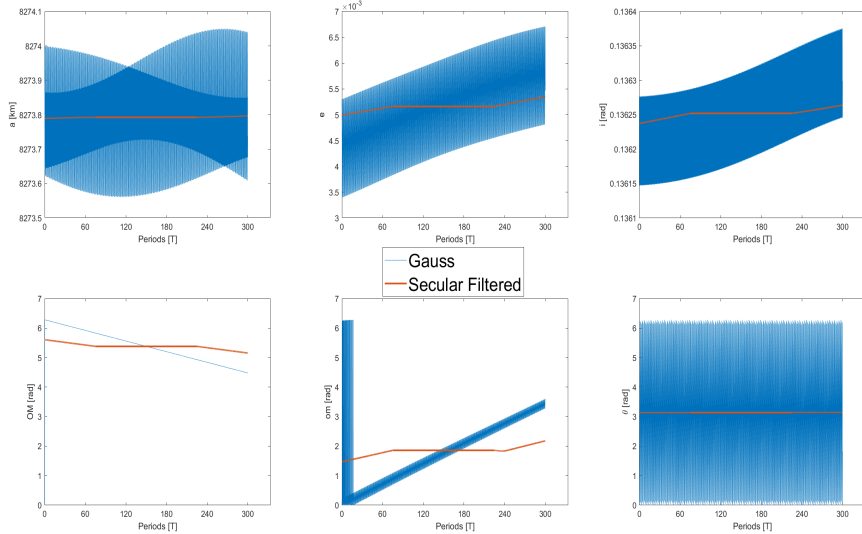


Figure 5.5: Filtering the Secular effect on Gauss Method With J_2 and SRP over $300 T_{orb}$

In order to achieve a more meaningful representation of the evolution of the orbital elements over time we needed to filter high frequencies which were produced in the computational analysis and raw numerical propagation. To do so the MATLAB command *Movemean* was used, performing in this case a low pass filter. *Movemean* returns an array of local k-point mean values, where each mean is calculated over a sliding window of length chosen at will.

The high frequencies could be detected over the length span of a T_{orb} , but in order to decrease boundary effects a greater time range needed to be set, bringing it to $2 T_{orb}$.

5.2 REAL ORBIT COMPARISON

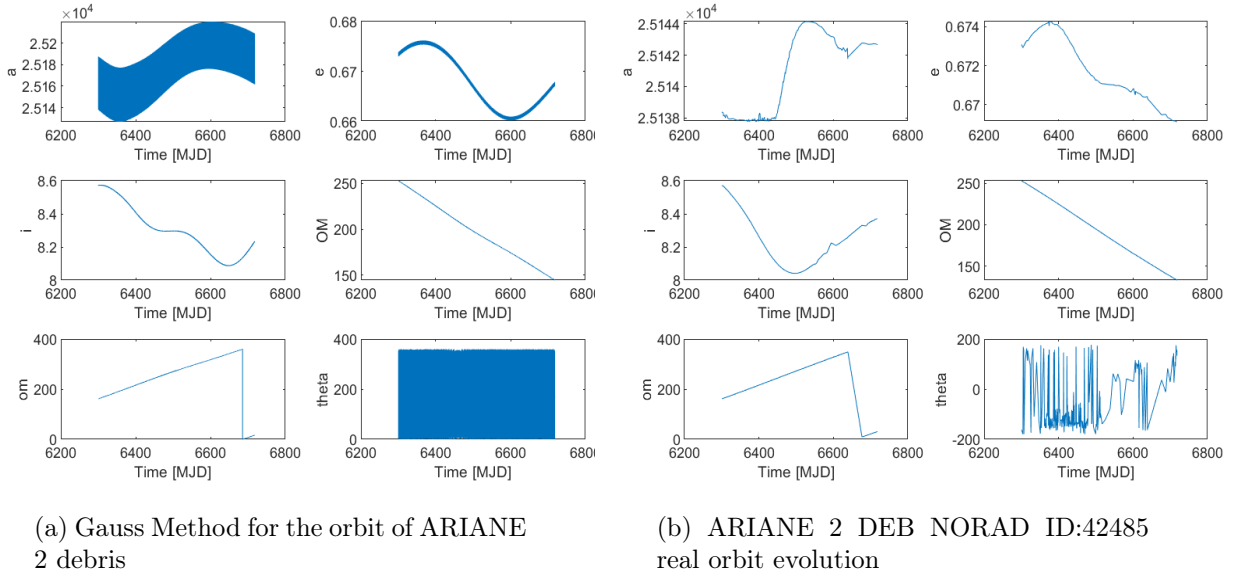


Figure 5.6: Accuracy of the Gauss with respect to the real evolution

The aim of this section is to compare the developed model, in this case the Gauss propagation method, with the real evolution of the satellite, downloaded by space track [2], in form of TLEs, and using the function that converts TLEs into Keplerian elements [3] revisited, to convert the TLEs in Keplerian elements.

The Orbit of ARIANE 2 Debris is an orbit similar to the one assigned, the difference are a and the e , but the radius of perigee and the inclination are almost the same, so the decision end up over this orbit because it is a "regular" orbit and the debris in this time span don't make maneuver

Little differences appears in every elements in particular in the *semi major axis* because the shape is almost the same, but the values are different, the real *semi major axis* remain in a more strict range of values. Other differences are clear in i this can be caused by the third body perturbation of the moon due to the high eccentricity and the the perigee very far from the Earth. The other elements like e , ω , Ω propagated by the model are very close to the real behavior due to the portion of the orbit in the same orbital region of the assigned orbit and hence subjected to the same perturbation.

Bibliography

- [1] Howard D. Curtis, text book, *Orbital Mechanics for Engineering students*, third edition, 2014.
- [2] Space-Track, web site, <https://www.space-track.org/#/gp>.
- [3] Brett Pantalone, Read Two-Line Element Ephemeris Files, 03/05/2016, Mathworks, <https://it.mathworks.com/matlabcentral/fileexchange/56904-read-two-line-element-ephemeris-files>.
- [4] A. Vallado, *Fundamentals of Astrodynamics and Applications (Space Technology Library)*. 4th Edition, Springer, 2007, Chapter 8.

6. APPENDIX A: PROCESS OUTPUT

DEPARTURE	ARRIVAL	FLYBY	$r_{pH}[km]$	$\Delta V[\text{km/s}]$
20-01-2050	28-07-2054	27-11-2056	3742.3558	38.3313
22-09-2042	23-08-2061	07-07-2065	3618.0180	29.8432
21-02-2035	03-05-2051	13-06-2060	3629.2758	37.5099
08-01-2035	10-08-2046	07-02-2054	3730.1930	30.0806
28-01-2057	02-01-2059	23-09-2060	3687.4644	39.5709
12-04-2035	13-03-2041	22-06-2043	3603.1053	31.5630
22-11-2051	21-08-2063	27-01-2066	3673.1405	27.9498
20-02-2035	31-01-2038	24-03-2048	3634.3594	40.2834
31-07-2046	08-05-2050	22-06-2053	3592.6302	24.6529
22-01-2047	10-04-2050	13-12-2052	3635.3480	26.8105
17-05-2045	06-05-2050	08-07-2053	6017.0340	24.9117
01-03-2041	02-05-2051	06-06-2060	3820.5487	36.1087
28-06-2039	13-02-2044	11-04-2050	3593.9761	43.4498
31-05-2031	15-06-2033	05-08-2054	3641.4122	41.3984
13-01-2048	13-08-2063	23-09-2065	3671.7156	29.0781
06-03-2037	27-05-2048	24-03-2053	3633.8244	29.8226
27-09-2046	23-12-2047	23-05-2051	3592.5677	50.5980
12-09-2040	24-12-2047	04-12-2049	3600.9850	41.7985
05-12-2030	10-02-2039	26-04-2054	3673.3643	32.6941
15-09-2043	03-07-2050	09-12-2054	3689.8880	27.4378
01-10-2048	06-05-2050	20-01-2054	3590.6216	33.2347
14-01-2041	15-02-2054	11-12-2065	10081.8438	31.7472
19-12-2029	29-05-2050	24-12-2053	3594.6579	29.5899
16-08-2058	21-08-2061	09-08-2065	3687.6476	27.5126
03-10-2028	17-12-2040	29-01-2054	6819.5054	31.9415
12-04-2035	21-03-2041	22-09-2043	3608.9992	33.3989
28-04-2047	29-05-2052	27-09-2054	3663.0629	25.5333

DEPARTURE	ARRIVAL	FLYBY	$r_{pH} [km]$	$\Delta V [km/s]$
03-12-2050	21-07-2055	02-04-2063	3832.0204	60.6232
20-06-2039	28-04-2049	25-09-2059	7278.8028	35.7865
02-03-2031	24-09-2044	09-01-2066	3697.1524	33.1779
05-06-2033	05-08-2033	09-03-2047	4211.1653	36.2649
06-05-2037	06-10-2038	09-08-2040	3591.5261	58.7578
29-03-2049	22-05-2050	17-10-2054	3602.5912	40.4249
01-04-2049	01-06-2052	09-11-2054	3659.5357	27.1212
01-01-2052	18-11-2056	21-06-2059	4250.2505	28.8217
01-02-2053	21-10-2059	25-01-2066	10241.750	28.4166
25-11-2047	14-11-2056	14-04-2059	3681.3536	31.4414
03-01-2045	01-02-2053	13-09-2059	8041.3962	33.8825
21-03-2040	02-04-2044	01-03-2051	3611.8665	49.0271
09-10-2031	02-05-2036	22-12-2048	3709.4487	41.6488
13-07-2037	10-08-2043	28-03-2047	3596.1893	30.1460
19-10-2053	21-10-2057	07-05-2065	3603.6370	32.2446
14-05-2029	17-07-2036	20-02-2050	3738.8695	47.6417
25-12-2055	07-08-2063	30-09-2065	3616.2165	26.6172
31-05-2051	21-01-2058	20-03-2067	3729.9391	32.9143
04-05-2030	26-07-2034	12-10-2036	3645.9344	30.2974
05-11-2059	30-08-2063	14-05-2066	3670.4678	24.6809
19-08-2045	30-06-2050	12-10-2054	3696.9231	26.4061
20-04-2047	02-10-2059	14-09-2065	3760.2649	29.9392
04-08-2036	16-09-2045	03-12-2047	3604.0216	32.2210
20-03-2040	27-12-2047	07-01-2050	3607.1291	42.3373
20-08-2058	18-08-2063	12-02-2066	7189.1264	24.7619
13-05-2059	25-09-2063	02-03-2067	4022.1754	28.1969
27-05-2031	20-09-2042	19-03-2053	3595.1364	33.5031
06-11-2035	07-04-2049	16-06-2059	5880.2291	35.7227
19-02-2032	13-07-2048	03-05-2066	11522.677	32.8787
27-02-2058	23-10-2061	04-02-2067	3951.2593	30.9170
17-12-2033	25-11-2051	31-10-2063	3609.9662	54.7194
28-01-2053	19-09-2059	26-05-2065	4708.2933	28.2342
30-01-2050	30-12-2056	16-02-2060	3625.7388	31.5813
22-02-2032	05-06-2035	21-02-2055	3700.1342	38.3692
29-08-2034	12-11-2041	19-02-2048	4593.7783	33.7522
17-06-2030	22-05-2037	26-07-2043	4002.2833	30.9093
17-10-2034	26-01-2043	21-11-2055	3655.4128	39.2940

DEPARTURE	ARRIVAL	FLYBY	$r_{pH} [km]$	$\Delta V [\text{km/s}]$
29-07-2033	16-05-2050	21-08-2053	3731.8971	29.0691
02-05-2033	14-12-2040	08-01-2054	3631.7324	32.3048
04-10-2032	28-10-2036	30-05-2039	3590.0500	44.7573
04-04-2052	22-02-2059	01-01-2061	3594.6692	36.7324
28-07-2049	02-11-2054	11-10-2058	3670.4469	29.6137
28-05-2038	17-08-2050	29-12-2055	3677.7292	40.3142
12-04-2038	13-11-2043	07-09-2048	3733.3469	32.7952
05-06-2057	12-08-2063	03-01-2066	3730.0134	25.3957
27-07-2043	10-01-2055	24-11-2059	3864.8116	34.3998
03-08-2046	23-01-2056	19-04-2066	6918.5500	30.7829
06-07-2051	29-08-2054	09-08-2057	3721.8009	36.8352
20-04-2034	03-02-2039	08-10-2041	8844.3953	24.4792
04-03-2034	20-11-2056	07-04-2059	3714.8820	34.1014
01-02-2056	07-04-2056	06-04-2059	3725.5930	28.8911
21-05-2055	06-01-2057	15-09-2060	3609.4984	39.4974
30-05-2031	03-02-2039	11-10-2041	3595.9594	26.2740
18-07-2054	03-09-2063	27-06-2066	3610.9167	27.4779
18-11-2058	20-09-2065	06-10-2067	3608.5627	41.1465
02-07-2055	12-12-2057	17-07-2066	3654.1868	35.3236
16-04-2061	11-09-2065	06-07-2067	3603.2979	37.8001
03-06-2044	04-06-2050	06-04-2054	6846.2739	26.0252
16-11-2045	12-08-2048	05-03-2055	3610.9442	33.9214
22-08-2041	06-02-2049	16-06-2058	3732.3984	42.0879
24-05-2051	24-09-2059	22-07-2065	3951.9436	28.7182
23-02-2045	04-01-2058	07-11-2066	3659.8942	30.9857
17-11-2058	21-08-2063	15-03-2066	6787.8960	24.6732
27-04-2060	19-09-2061	23-10-2066	3704.0873	38.2820
04-07-2032	28-06-2034	05-09-2036	3595.3937	34.7157
29-12-2051	03-11-2056	23-02-2059	4832.5523	28.5330
22-02-2032	26-01-2058	17-04-2067	3778.1772	35.0148
07-09-2040	06-08-2051	13-12-2061	3735.9891	45.1773
23-01-2030	21-12-2052	23-12-2058	3720.9896	35.5732
06-05-2036	21-01-2038	26-03-2048	3594.3244	44.8998
03-11-2049	07-04-2055	18-04-2061	3619.0671	38.2591
20-05-2035	05-05-2051	23-06-2060	3634.5169	37.5544
05-12-2053	24-11-2056	23-05-2059	3602.3563	29.0729

Table 6.1: output of the GA algorithm

7. APPENDIX B: SURF PLOT OF THE INTERPLANETARY LEGS

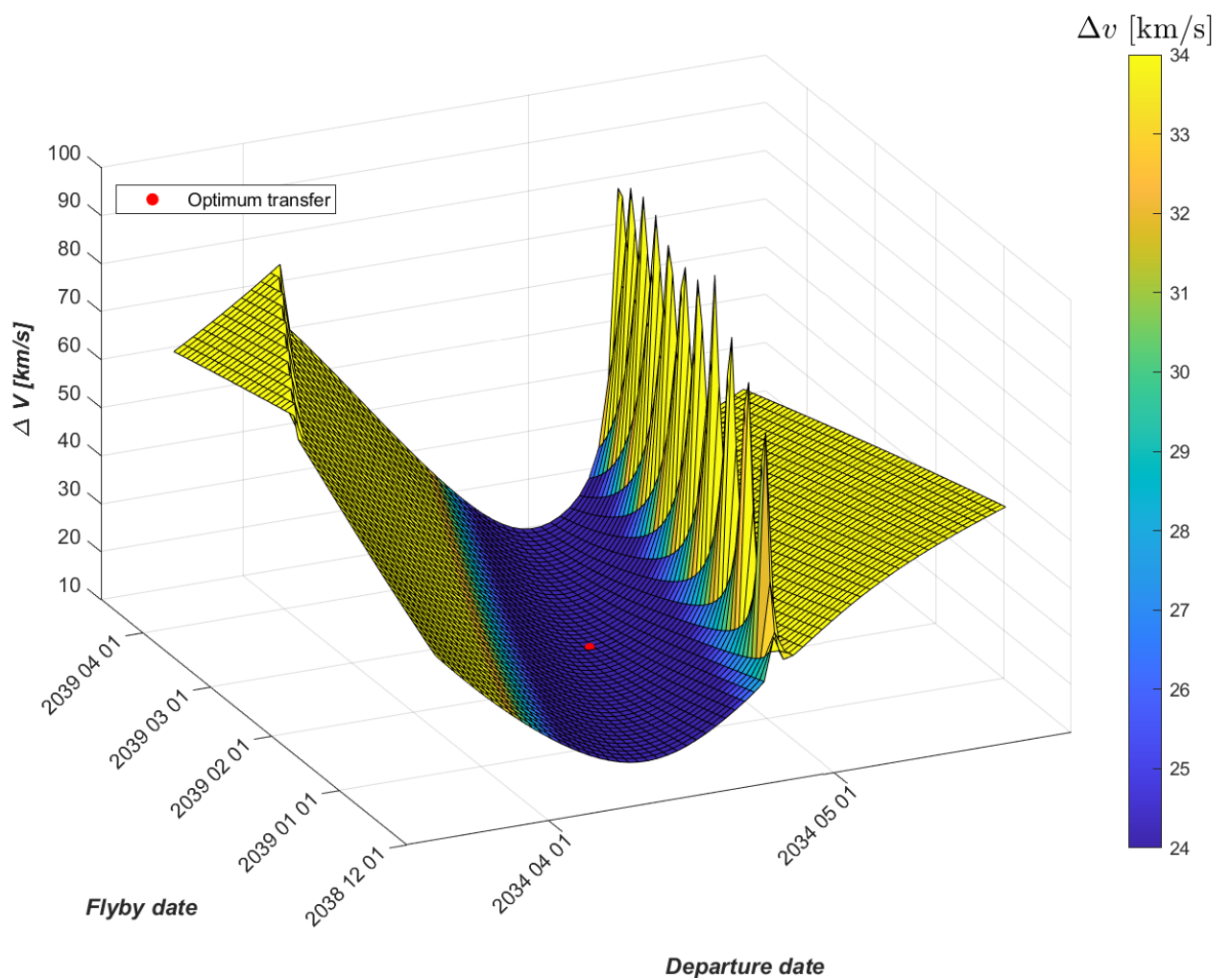


Figure 7.1: Surf plot of the first leg

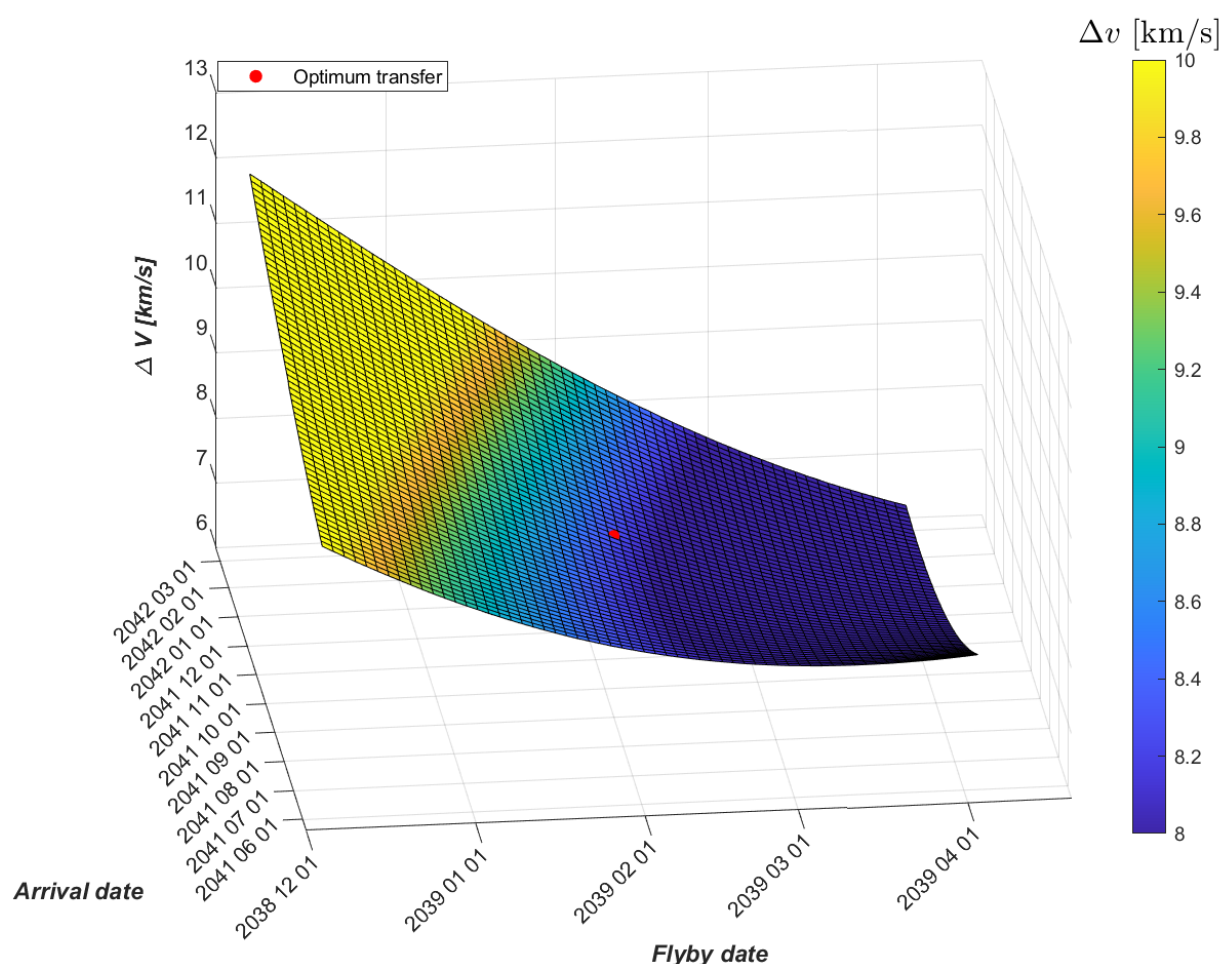


Figure 7.2: Surf plot of the second leg